Article

Cell Reports

Structural Insights into How Yrb2p Accelerates the Assembly of the Xpo1p Nuclear Export Complex

Graphical Abstract

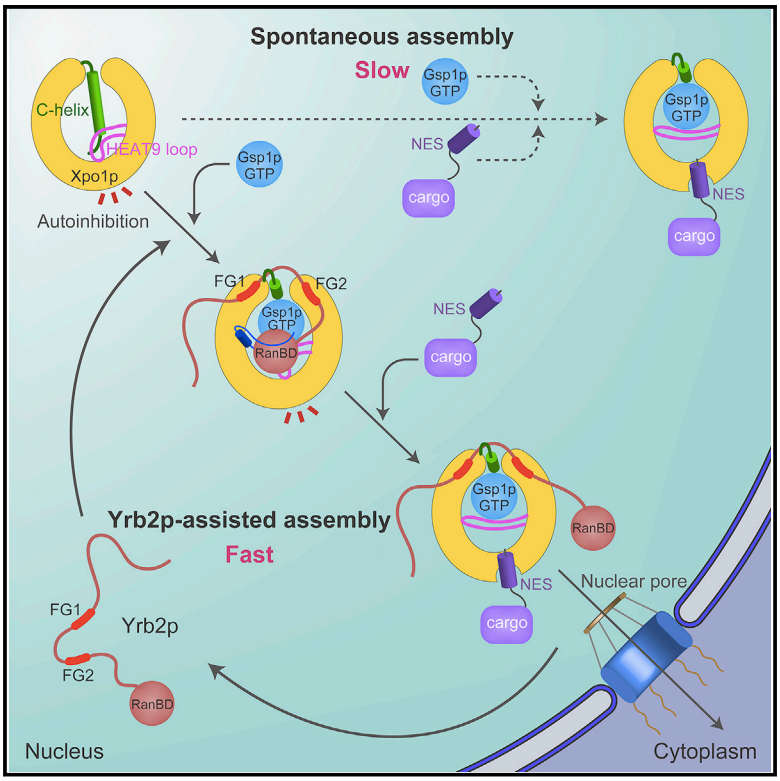

Authors

Masako Koyama, Natsuki Shirai, Yoshiyuki Matsuura

Correspondence

matsuura.yoshiyuki@d.mbox.nagoya-u.ac.jp

In Brief

Koyama et al. now look at how the Ran-binding protein Yrb2p (yeast RanBP3) promotes nuclear export of proteins and ribonucleoproteins. Yrb2p strikingly increases the rate of cargo loading onto the nuclear export receptor Xpo1p (yeast CRM1) through an allosteric mechanism.

Highlights

Yrb2p increases the association rate of Gsp1p-GTP and NES with Xpo1p

The crystal structure of Xpo1p-Yrb2p-Gsp1p-GTP complex is determined

Yrb2p primes Xpo1p and Gsp1p for rapid loading of NES by an allosteric mechanism

The structure also reveals the major FG-repeat binding sites on Xpo1p

Accession Numbers

3WYF
3WYG

Koyama et al., 2014, Cell Reports 9, 983–995
November 6, 2014 ©2014 The Authors
http://dx.doi.org/10.1016/j.celrep.2014.09.052

Cell Reports
Article

Structural Insights into How Yrb2p Accelerates the Assembly of the Xpo1p Nuclear Export Complex

Masako Koyama,[1] Natsuki Shirai,[1] and Yoshiyuki Matsuura[1,2,*]
[1]Division of Biological Science
[2]Structural Biology Research Center
Graduate School of Science, Nagoya University, 464-8602 Furo-cho, Chikusa-ku, Nagoya City, Japan
*Correspondence: matsuura.yoshiyuki@d.mbox.nagoya-u.ac.jp
http://dx.doi.org/10.1016/j.celrep.2014.09.052

SUMMARY

Proteins and ribonucleoproteins containing a nuclear export signal (NES) assemble with the exportin Xpo1p (yeast CRM1) and Gsp1p-GTP (yeast Ran-GTP) in the nucleus and exit through the nuclear pore complex. In the cytoplasm, Yrb1p (yeast RanBP1) displaces NES from Xpo1p. Efficient export of NES-cargoes requires Yrb2p (yeast RanBP3), a primarily nuclear protein containing nucleoporin-like phenylalanine-glycine (FG) repeats and a low-affinity Gsp1p-binding domain (RanBD). Here, we show that Yrb2p strikingly accelerates the association of Gsp1p-GTP and NES to Xpo1p. We have solved the crystal structure of the Xpo1p-Yrb2p-Gsp1p-GTP complex, a key assembly intermediate that can bind cargo rapidly. Although the NES-binding cleft of Xpo1p is closed in this intermediate, our data suggest that preloading of Gsp1p-GTP onto Xpo1p by Yrb2p, conformational flexibility of Xpo1p, and the low affinity of RanBD enable active displacement of Yrb2p RanBD by NES to occur effectively. The structure also reveals the major binding sites for FG repeats on Xpo1p.

INTRODUCTION

Rapid exchange of macromolecules between the nucleus and the cytoplasm is a crucial cellular function that regulates many physiological processes. Nuclear transport proceeds through nuclear pore complexes (NPCs), a large protein assembly embedded in the nuclear envelope. The NPC is equipped with a barrier that is freely permeable for small molecules but suppresses the flux of large objects >5 nm in diameter (Mohr et al., 2009) unless they are bound by cognate nuclear transport receptors (NTRs). The NTRs circulate rapidly between the nucleus and the cytoplasm and transfer cargoes from one side of the nuclear envelope to the other (reviewed in Görlich and Kutay, 1999). The NPC is composed of multiple copies of about 30 different protein subunits (nucleoporins or nups) (Rout et al., 2000; Cronshaw et al., 2002). About one-third of these nups contain tandem sequence repeats, so-called phenylalanine-glycine (FG) repeats, based on short hydrophobic cores containing phenylalanine and glycine residues, typically of the sequence FG, FxFG, (where x is usually a small residue), or GLFG, separated by linkers of variable sequence and length. The FG repeat domains represent natively unfolded, nonglobular protein structures (Denning et al., 2003) that are essential for viability and are involved in forming the permeability barrier in the central channel of the NPC (Strawn et al., 2004; Frey and Görlich, 2007; Patel et al., 2007; Hülsmann et al., 2012). All known NTRs can bind to FG-nups, and interactions between the FG repeats and NTRs are essential for NTR-cargo complexes to penetrate the barrier (reviewed in Stewart et al., 2001; Stewart, 2007). The NPC passage of NTR-cargo complexes is reversible (Nachury and Weis, 1999), and the active cargo release in the destination compartment is important to drive transport in one direction.

In *Saccharomyces cerevisiae*, Xpo1p (CRM1 in vertebrates) is a major NTR that mediates nuclear export of a broad range of cargo macromolecules containing the leucine-rich nuclear export signal (NES) (Fornerod et al., 1997; Fukuda et al., 1997; Ossareh-Nazari et al., 1997; Stade et al., 1997). Cargo loading and release is guided by a concentration gradient of Gsp1p-GTP (Ran-GTP in vertebrates) across the nuclear envelope. A high nuclear Gsp1p-GTP concentration favors cargo loading onto Xpo1p in the nucleus, whereas cytoplasmic Ran-binding proteins Yrb1p and Rna1p (RanBP1 and RanGAP in vertebrates) promote cargo release from Xpo1p and GTP hydrolysis by Gsp1p in the cytoplasm. In this respect, each of the four Ran-binding domains (RanBDs) of RanBP2 in vertebrates functions similarly to RanBP1. Recent crystallographic studies have defined the cooperative interactions between Xpo1p (CRM1), NES, and Gsp1p-GTP (Ran-GTP) (Dong et al., 2009; Monecke et al., 2009; Güttler et al., 2010; Saito and Matsuura, 2013; Monecke et al., 2013). Xpo1p (CRM1) is a toroid-shaped molecule that is constructed from 21 tandem HEAT repeats, each of which consists of two antiparallel α helices, designated A helix and B helix. The A helices form outer convex surface, whereas the B helices form the inner concave surface. NES binds to the hydrophobic cleft on the outer surface of Xpo1p (CRM1), formed between the A helices of HEAT repeats 11 and 12, whereas Gsp1p-GTP (Ran-GTP) binds to the interior surface of Xpo1p (CRM1), making intimate contacts with HEAT repeats 1–4, 17, and 19 and a long β hairpin loop (referred to as HEAT9 loop) inserted between the A and B helices of HEAT repeat 9. HEAT9

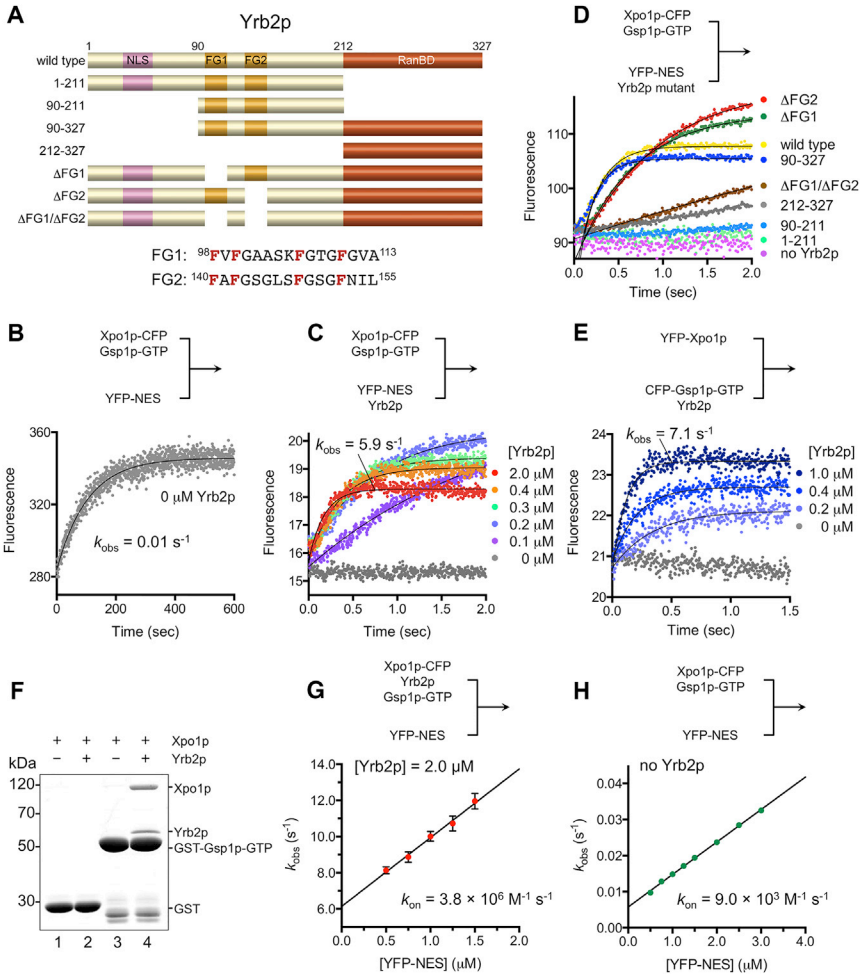

Figure 1. Yrb2p Accelerates the Association of NES and Gsp1p-GTP to Xpo1p

(A) Domain organization of Yrb2p.

(B–E) Stopped-flow traces. CFP was excited at 430 nm, and YFP emission was monitored. In (B) and (C), a solution of 0.2 μM Xpo1p-CFP and 3.0 μM Gsp1p-GTP was rapidly mixed with a solution of 1.0 μM YFP-NES and 0.0–2.0 μM Yrb2p. In (D), a solution of 0.2 μM Xpo1p-CFP and 3.0 μM Gsp1p-GTP was rapidly mixed with a solution of 1.0 μM YFP-NES and 0.5 μM Yrb2p. In (E), a solution of 0.5 μM YFP-Xpo1p was rapidly mixed with a solution of 0.5 μM CFP-Gsp1p-GTP and 0.0–1.0 μM Yrb2p.

(F) GST pull-down assay. Immobilized GST (44 μg; lanes 1 and 2) or GST-Gsp1p-GTP (82 μg; lanes 3 and 4) was incubated with Xpo1p (30 μg) with or without Yrb2p (50 μg).

(G) A solution of 0.2 μM Xpo1p-CFP, 2.0 μM Yrb2p, and 3.0 μM Gsp1p-GTP was rapidly mixed with a solution of 0.5–1.5 μM YFP-NES. The observed association rates were plotted against concentration of YFP-NES. The straight line gives a second-order association rate constant k_{on} of 3.8 × 10^6 $M^{-1}s^{-1}$. Error bars represent standard errors (n = 3).

(H) A solution of 0.2 μM Xpo1p-CFP and 3.0 μM Gsp1p-GTP was rapidly mixed with a solution of 0.5–3.0 μM YFP-NES. The observed association rates were plotted against concentration of YFP-NES. The straight line gives a second-order association rate constant k_{on} of 9.0 × 10^3 $M^{-1}s^{-1}$. Error bars represent SE (n = 3).

See also Figure S1.

loop plays a key role in the cooperative Gsp1p-GTP (Ran-GTP) and cargo binding to Xpo1p (CRM1) (Koyama and Matsuura, 2010; Saito and Matsuura, 2013). In free Xpo1p (CRM1), HEAT9 loop binds to the inner surface beneath the NES-binding cleft, stabilizing the cleft in a closed conformation that is incompatible with cargo binding. This autoinhibitory activity of HEAT9 loop is reinforced by the C-terminal tail of Xpo1p (CRM1) (Saito and Matsuura, 2013). The binding of Gsp1p-GTP (Ran-GTP) to Xpo1p (CRM1) is associated with movement of the C terminus and HEAT9 loop of Xpo1p (CRM1), allowing for opening of the NES-binding cleft and binding of cargo (Saito and Matsuura, 2013). The cytoplasmic protein Yrb1p (RanBP1 or RanBP2) utilizes the autoinhibitory activity of HEAT9 loop to accelerate cargo release (Koyama and Matsuura, 2010). Association of the RanBD of Yrb1p (RanBP1 or RanBP2) to the Xpo1p -NES-Gsp1p-GTP (CRM1-NES-Ran-GTP) complex in the cytoplasm induces movement of HEAT9 loop to the autoinhibitory position (the concave side of the NES-binding cleft). This results in closure of the hydrophobic cleft to dissociate NES (Koyama and Matsuura, 2010). The idea that HEAT9 loop has an important mechanistic role in controlling the conformational dynamics of Xpo1p (CRM1) has been supported by a recent molecular dynamics simulation study (Dölker et al., 2013).

Crystallographic studies of Xpo1p (CRM1) so far have advanced understanding of how transport directionality is controlled, especially in terms of how Gsp1p-GTP (Ran-GTP) stabilizes cargo binding and how RanBDs in the cytoplasm facilitate cargo release and highlighted HEAT9 loop as a primary determinant of the conformation of the NES-binding site. Nevertheless, there are issues still unresolved, including the structural basis for the function of Xpo1p (CRM1)-specific cofactors in nuclear export. Although it has been known for more than a decade that efficient export of NES-cargoes in *S. cerevisiae* requires a primarily nuclear Gsp1p (Ran)-binding protein Yrb2p (RanBP3 in vertebrates) (Taura et al., 1998; Noguchi et al., 1999), the mechanism of action of Yrb2p (RanBP3) remains poorly understood. Yrb2p has a multidomain structure based on an N-terminal domain containing a nuclear localization signal (NLS), a central domain containing FG repeats that bind Xpo1p specifically, and a C-terminal Gsp1p-binding domain (RanBD) that is homologous to Yrb1p (RanBP1) (Dingwall et al., 1995) (Figure 1A). However, Yrb2p binds Gsp1p-GTP only extremely weakly (Noguchi et al., 1997), unlike Yrb1p (RanBP1) or RanBP2 that binds Gsp1p-GTP (Ran-GTP) with high affinity (Kuhlmann et al., 1997) and functions as a cytoplasmic disassembly factor for the Xpo1p (CRM1) nuclear export complex (Koyama and Matsuura, 2010). Yeast cells deleted for the *YRB2* gene are cold sensitive (Noguchi et al., 1997; Taura et al., 1997) and

show severe defect in Xpo1p-mediated nuclear export (Taura et al., 1998; Noguchi et al., 1999). Yrb2p interacts with the Gsp1p nucleotide exchange factor Prp20p (yeast RCC1), and *yrb2Δ* is synthetically lethal with temperature-sensitive mutants of *prp20* (Taura et al., 1997). Hba1p, the fission yeast ortholog of Yrb2p (Noguchi et al., 1999), is essential for viability (Turi et al., 1996). RanBP3, the human ortholog of Yrb2p, has a multidomain structure similar to that of Yrb2p and stimulates CRM1 export pathway in permeabilized cells (Englmeier et al., 2001; Lindsay et al., 2001).

The cooperative binding of cargo and Ran-GTP to CRM1 has been suggested to be the most rate-limiting step in nuclear export (Kehlenbach et al., 2001) and could be the point of regulation by cofactors. Generally, the assembly of macromolecular complexes depends on diffusion-driven, random collision of subunits. The diffusion rates amidst the high concentrations of biological macromolecules in living cells are much reduced than those in the uncrowded buffers in vitro (Ellis, 2001), and efficient assembly of macromolecular complexes in vivo often requires assisting factors referred to as assembly chaperones (Ellis, 2006; Chari and Fischer, 2010). Yrb2p (RanBP3) may play such an assisting role in the Xpo1p (CRM1)-mediated export pathway because it has been shown that RanBP3 increases the affinity of CRM1 for NES and Ran-GTP when RanBP3 is present at an optimal concentration (Englmeier et al., 2001; Lindsay et al., 2001). However, the pull-down assays and RanGAP protection assays used in the previous studies (Englmeier et al., 2001; Lindsay et al., 2001) cannot directly measure the rates of protein-protein association, and so it remains unclear how Yrb2p (RanBP3) affects the assembly kinetics of the Xpo1p (CRM1) nuclear export complex. It was also puzzling that too much RanBP3 inhibits the binding of CRM1 and Ran-GTP to NES (Englmeier et al., 2001) and that overexpression of Yrb2p (RanBP3) (or microinjection of too much RanBP3 into the nucleus) inhibits NES-protein export in vivo (Taura et al., 1998; Englmeier et al., 2001; Sabri et al., 2007). To dissect the mechanism of action of Yrb2p (RanBP3), we performed detailed structural and functional characterization of the interactions between Xpo1p, Yrb2p, Gsp1p, NES, and FG-nups in this study. Here we show direct evidence that Yrb2p dramatically increases the rate of association of Gsp1p-GTP and NES to Xpo1p and also report the crystal structure of a key intermediate (Xpo1p-Yrb2p-Gsp1p-GTP complex) in the assembly reaction of the Xpo1p nuclear export complex. Although the architecture of this assembly intermediate was unexpectedly similar to that of Xpo1p-Yrb1p-Gsp1p-GTP complex, the atomic details of interactions and structure-based functional analyses provided clear mechanistic insights that Yrb1p and Yrb2p exploit Xpo1p allostery in different ways to perform entirely different functions. The structure also provided a structural view of how Xpo1p interacts with the FG-repeat motif.

RESULTS AND DISCUSSION

Yrb2p Accelerates Association of Gsp1p-GTP and NES to Xpo1p

We previously showed that the RanBD of Yrb1p (RanBP1/2) increases the off-rate of NES from Xpo1p (CRM1) and Gsp1p-GTP (Ran-GTP) by using a real-time assay based on fluorescence resonance energy transfer (FRET) that monitors the binding of NES to Xpo1p (CRM1) (Koyama & Matsuura, 2010). In the present study, we used this FRET-based assay to examine how Yrb2p might affect the on-rate of NES. Association kinetics of NES binding to Xpo1p were measured by monitoring the increase in the FRET signal between Xpo1p-CFP and YFP-NES in the presence of Gsp1p-GTP and increasing concentrations of Yrb2p in a stopped-flow apparatus. Yrb2p remarkably accelerated NES association in the presence of Gsp1p-GTP (Figures 1B and 1C; Table S1). This activity of Yrb2p required two clusters of FG repeats (referred to as FG1 and FG2, as defined in Figure 1A) in the central domain and the C-terminal RanBD, but did not require the N-terminal domain (Figure 1D). This parallels the previous observation that both FG-repeat domain and RanBD are required for full activity of Yrb2p and RanBP3 to promote nuclear export (Taura et al., 1998; Lindsay et al., 2001). Yrb2p also remarkably accelerated association of Gsp1p-GTP to Xpo1p (Figure 1E), forming a stable ternary complex that was readily detectable by a pull-down assay (Figure 1F). In contrast, the binding of Xpo1p alone to Gsp1p-GTP was hardly detectable (Figure 1F). The NES association rates obtained by rapidly mixing the preformed ternary complex (Xpo1p-CFP bound to Yrb2p and Gsp1p-GTP) with increasing concentrations of YFP-NES were plotted against the YFP-NES concentration to obtain k_{on} of 3.8×10^6 $M^{-1}s^{-1}$ (Figure 1G), which was two orders of magnitude faster than the k_{on} (9.0×10^3 $M^{-1}s^{-1}$) of NES binding to Xpo1p in the presence of a large excess of Gsp1p-GTP (but in the absence of Yrb2p) (Figure 1H). Taken together, our data suggest that Yrb2p accelerates the initial step of nuclear export by recruiting Gsp1p-GTP to Xpo1p to form an intermediate complex that can bind cargo rapidly in the nucleus. Kinetic measurements also indicated that human RanBP3, like yeast Yrb2p, accelerates the assembly of the CRM1 nuclear export complex (Supplemental Results and Discussion; Figure S1).

Overall Structure of Xpo1p-Yrb2p-Gsp1p-GTP Complex: A Key Assembly Intermediate that Can Bind Cargo Rapidly

To understand the structural basis for how Yrb2p increases the on-rates of Gsp1p-GTP and NES-cargo to Xpo1p, we crystallized the key intermediate complex (Xpo1p-Yrb2p-Gsp1p-GTP complex). We used the construct of Yrb2p (residues 90–327) that encompasses both FG-repeat domain and RanBD and retains the activity of full-length Yrb2p to accelerate assembly of the Xpo1p nuclear export complex (Figure 1D; Table S1). The structure was solved at 2.22 Å resolution (Figure 2A; Table S2). The crystals contained two complexes per asymmetric unit, with essentially identical structures (C_α root mean square deviation of 0.72 Å). To enable a complete comparison to be made between different conformations of Xpo1p, we also determined the structure of Xpo1p bound to PKI (a representative NES-cargo; Wen et al., 1995) and Gsp1p-GTP at 2.15 Å resolution (Figure 2B; Table S2). Unlike previous structural studies on CRM1 (Güttler et al., 2010), this structure of cargo-bound Xpo1p was determined without artificially fusing NES to the C-terminal domain of snurportin and confirmed that Xpo1p recognizes the PKI

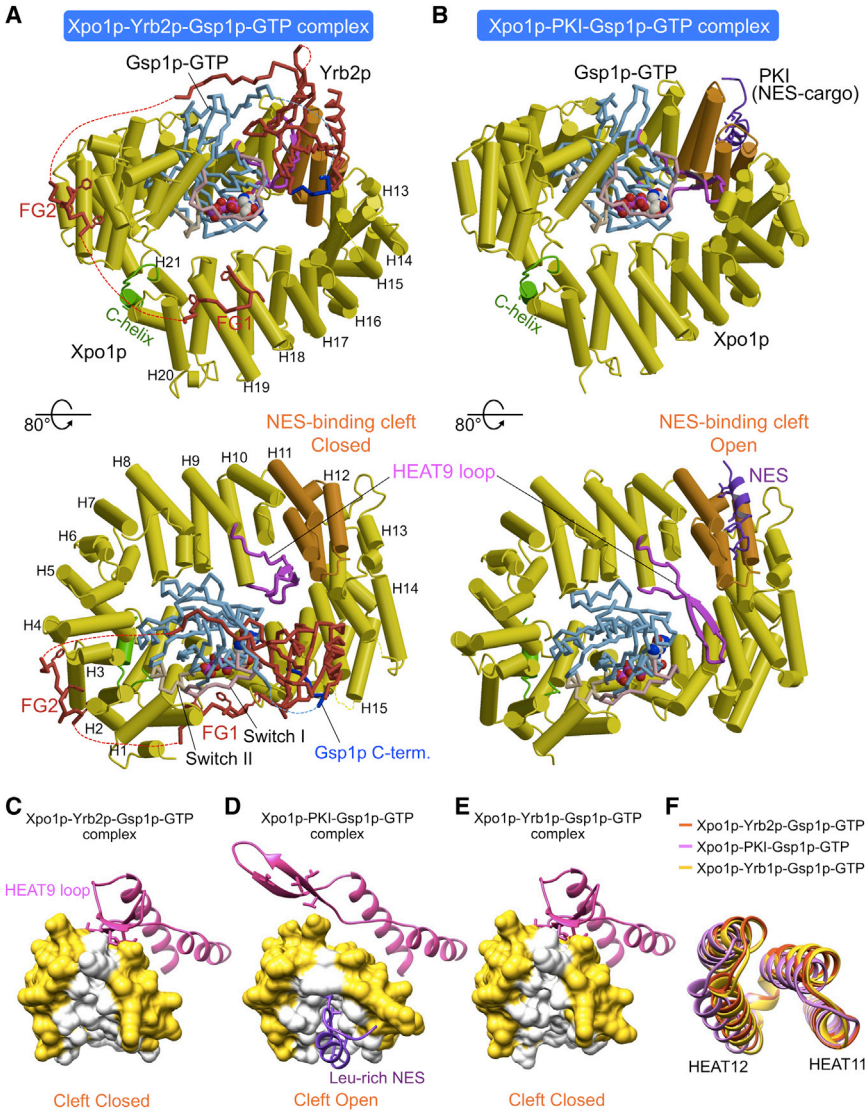

Figure 2. Structures of an Assembly Intermediate and the Fully Assembled Xpo1p Nuclear Export Complex

(A) Xpo1p-Yrb2p-Gsp1p-GTP complex. The HEAT repeats of Xpo1p are labeled H1-H21. Xpo1p is colored yellow, except that HEAT9 loop, HEAT repeats 11 and 12 (that constitute the NES-binding site), and the C-terminal region beyond the A helix of HEAT21 are highlighted in magenta, orange, and light green, respectively. Gsp1p is colored cyan, with its switch I, switch II, and the C-terminal tail highlighted in pink, gray, and blue, respectively. Yrb2p is colored red, with its phenylalanine side chains of FG1 and FG2 shown in stick representation.

(B) Xpo1p-PKI-Gsp1p-GTP complex. PKI is colored purple. The hydrophobic side chains of the NES are shown in stick representation.

(C–E) The conformation of the NES-binding cleft of Xpo1p-Yrb2p-Gsp1p-GTP complex (C), Xpo1p-PKI-Gsp1p-GTP complex (D), and Xpo1p-Yrb1p-Gsp1p-GTP complex (E). The closed conformation of this cleft is stabilized by interaction between the HEAT9 loop (magenta) and the inner surface of Xpo1p immediately behind the NES-binding cleft. This cleft is open in Xpo1p-PKI-Gsp1p-GTP complex and accommodates hydrophobic side chains of NES (purple). The HEAT repeats 11 and 12 are shown in surface representation, and the residues that directly interact with NES are colored white, whereas the other residues are colored yellow.

(F) Superposition of HEAT repeats 11 and 12 of Xpo1p-Yrb2p-Gsp1p-GTP complex (orange), Xpo1p-PKI-Gsp1p-GTP complex (pink), and Xpo1p-Yrb1p-Gsp1p-GTP complex (yellow). Orientation is the same as (C–E).

See also Figure S2.

NES in essentially the same way as observed previously in the structure of mouse CRM1 bound to Ran-GTP and NES-snurportin chimera (Güttler et al., 2010).

FG1 and FG2 had unambiguously clear electron density in the crystal of the Yrb2p complex and bound to the outer surface of Xpo1p at HEAT repeats18–20 and HEAT repeats 2–4, respectively (Figures S2A and S2B). RanBD bound on top of Gsp1p. The linker between FG1 and FG2 and the linker between FG2 and RanBD did not have defined electron density, and so it was not possible to establish unequivocally that the bound FG1, FG2, and RanBD came from the same chain of Yrb2p rather than from adjacent molecules in the crystal. However, the linkers are sufficiently long to connect FG1, FG2, and RanBD, as indicated by the red dashed lines in Figure 2A, and so the crystal structure supports the idea that Yrb2p functions as a scaffold to recruit Gsp1p-GTP to Xpo1p. The structure is also consistent with previous biochemical data that indicated that RanBP3 does not increase the stoichiometry of Ran-GTP binding to CRM1 and instead acts by increasing the affinity of CRM1-RanBP3 complex for Ran-GTP (Lindsay et al., 2001).

The overall architecture of Xpo1p-Yrb2p-Gsp1p-GTP complex was similar to that of Xpo1p-Yrb1p-Gsp1p-GTP complex (Figures 2A and S2C), and as observed in the Yrb1p complex (Koyama and Matsuura, 2010), the arrangements of RanBD and HEAT9 loop were such that the NES-binding cleft in Xpo1p-Yrb2p-Gsp1p-GTP complex is in a closed conformation, which was distinct from an open conformation observed in the PKI complex (Figures 2C–2F). This is consistent with the fact that too much RanBP3 outcompetes NES in the binding to CRM1 and Ran-GTP (Englmeier et al., 2001), but on the other hand raises an intriguing question as to how Yrb2p accelerates NES association, in contrast to Yrb1p that accelerates NES dissociation. Close examination of the details of RanBD interactions gave an important clue to solve this puzzle.

Weak RanBD Interactions in Xpo1p-Yrb2p-Gsp1p-GTP Complex

Although the RanBDs of Yrb1p and Yrb2p have the same fold (Figures S3A and S3B), the low sequence identity (only

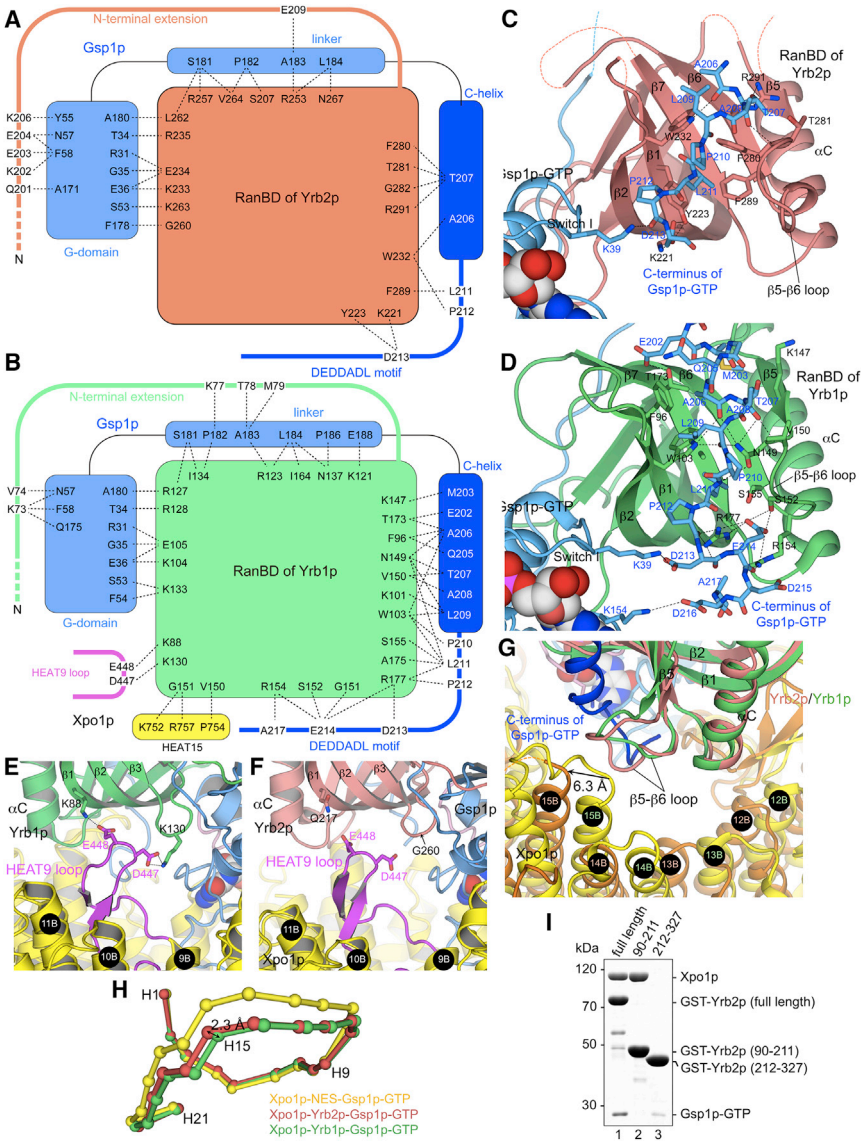

Figure 3. RanBD Interactions

(A and B) Schematic illustrations depicting the interactions involving RanBDs. (A) Xpo1p-Yrb2p-Gsp1p-GTP complex. (B) Xpo1p-Yrb1p-Gsp1p-GTP complex. Intermolecular contacts are shown as dotted lines. The contacting residues are defined as those having an interresidue distance below the cutoff of 3.6 Å.

(C and D) Interactions involving the C terminus of Gsp1p. (C) Xpo1p-Yrb2p-Gsp1p-GTP complex. (D) Xpo1p-Yrb1p-Gsp1p-GTP complex. Gsp1p (cyan) and the RanBD of Yrb2p (dark pink) and Yrb1p (green) are shown as ribbon models, except for Gsp1p C terminus shown as stick models. Key residues of RanBDs interacting with Gsp1p C terminus are shown as stick models. Dotted lines indicate hydrogen bonds or salt bridges.

(E and F) RanBD-HEAT9 loop interactions (salt bridges, indicated by dotted lines) are observed in Xpo1p-Yrb1p-Gsp1p-GTP complex (E) but not in Xpo1p-Yrb2p-Gsp1p-GTP complex (F). HEAT9 loop is colored magenta.

(G) Overlay of Xpo1p (yellow)-Yrb1p (green)-Gsp1p-GTP complex and Xpo1p (orange)-Yrb2p (dark pink)-Gsp1p-GTP complex, illustrating loss of RanBD-HEAT15 contact in the Yrb2p complex. Gsp1p is colored cyan, except for its C terminus, which is colored blue (only Gsp1p in the Yrb1p complex is shown).

(H) Change in superhelical paths of Xpo1p HEAT repeats. The centers of consecutive HEAT repeats are represented by spheres. The yellow is Xpo1p in Xpo1p-PKI-Gsp1p-GTP complex. The dark pink is Xpo1p in Xpo1p-Yrb2p-Gsp1p-GTP complex, and green is Xpo1p in Xpo1p-Yrb1p-Gsp1p-GTP complex. HEAT1, 9, 15, and 21 are labeled H1, H9, H15, and H21, respectively.

(I) GST pull-down assay. Immobilized 1.3 nmol of GST-Yrb2p (full-length) (lane 1) or GST-Yrb2p (residues 90–211; the FG-repeat domain) (lane 2) or GST-Yrb2p (residues 212–327; the RanBD) (lane 3) was incubated with Xpo1p (30 μg) and Gsp1p-GTP (50 μg).

See also Figure S3.

30%; Figure S3C) of these RanBDs resulted in substantial differences in RanBD interactions with Gsp1p and Xpo1p (Figures 3 and S3C; Tables S3 and S4). In both Xpo1p-Yrb1p-Gsp1p-GTP complex and Xpo1p-Yrb2p-Gsp1p-GTP complex, RanBD and Gsp1p embrace each other (Figures 3A and 3B): the globular guanine-nucleotide binding domain (G domain), the linker, and the C terminus (the C helix and the acidic D-E-D-D-A-D-L motif) of Gsp1p wrap around the pleckstrin-homology (PH) domain of RanBD, and the N-terminal extension of RanBD reaches across the G-domain of Gsp1p. Most of the RanBD residues (on the β strands β2, β3, and β4) that contact the G domain of Gsp1p are conserved (Figure S3C), and the RanBD contact area for the G domain and the linker of Gsp1p in the Yrb2p complex (1120 Å^2) is only slightly smaller than that in the Yrb1p complex (1294 Å^2). However, the RanBD residues at the interface to the C terminus of Gsp1p, formed by the β strands β1, β2, β5, β6, and the β5–β6 loop of RanBD, are less well conserved (Figure S3C), disrupting this interface substantially in the Yrb2p complex. The crystallographic electron density suggested that this disruption of the interface resulted in weaker binding of the Gsp1p C terminus in the Yrb2p complex relative to the Yrb1p complex: only residues 203–213 of the C terminus of Gsp1p had electron density that was strong enough to be traced reliably in the Yrb2p complex, in contrast to the Yrb1p complex, in which residues 197–217 of the C terminus of Gsp1p had well-defined density. Consequently, much less contacts are made between Yrb2p and Gsp1p C terminus compared with Yrb1p-Gsp1p interactions (Figures 3A–3D), and the RanBD contact area for the C terminus of Gsp1p in the Yrb2p complex (482 Å^2) was ~2-fold smaller than that in the Yrb1p complex (898 Å^2). Thus, the RanBD interactions with the C terminus of Gsp1p (Ran), which are known to make a key contribution to the binding of RanBD

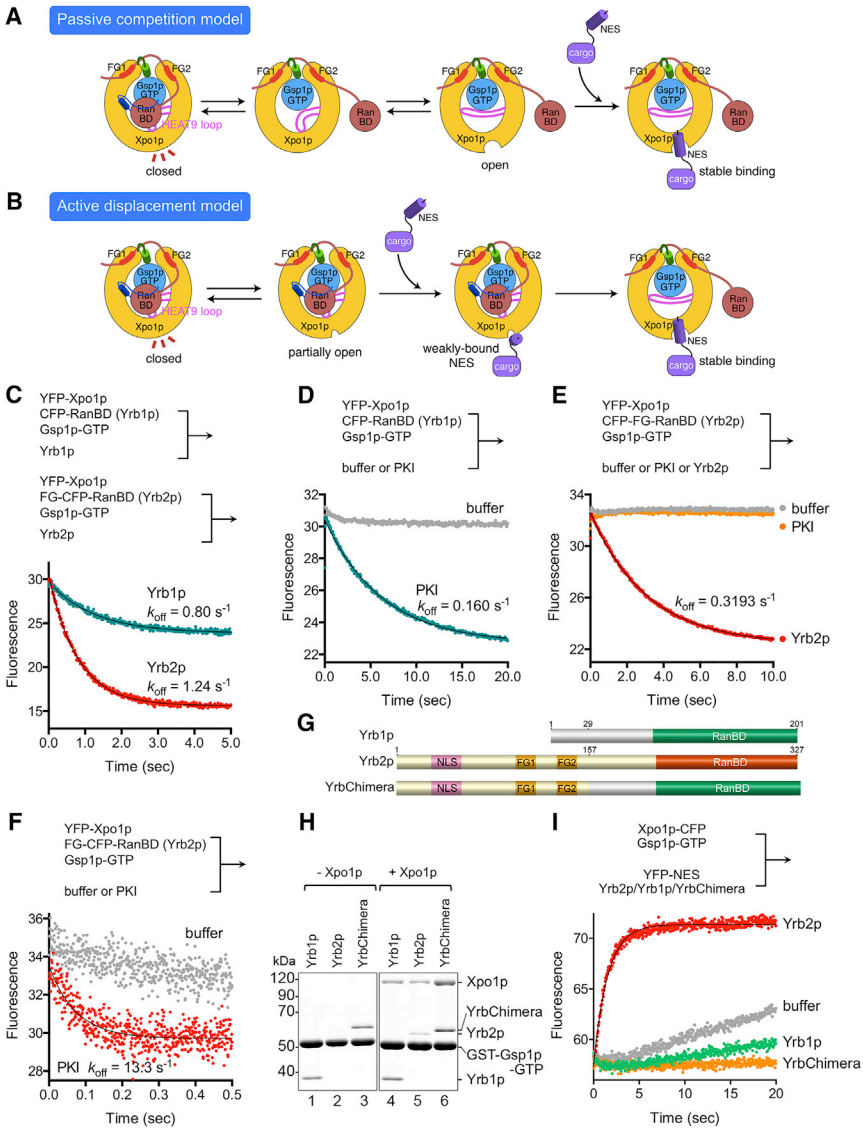

Figure 4. NES Actively Displaces RanBD of Yrb2p

(A and B) Passive competition model (A) and active displacement model for the competition between NES and RanBD of Yrb2p (B). See the text for details. HEAT9 loop is colored magenta.

(C–F) Stopped-flow traces. CFP was excited at 430 nm, and YFP emission was monitored. A solution of 0.2 μM YFP-Xpo1p, 0.2 μM CFP-RanBD (Yrb1p), and 4.0 μM Gsp1p-GTP was rapidly mixed with either 4.0 μM Yrb1p (C), buffer alone, or 20 μM PKI (S35L) (D). A solution of 0.2 μM YFP-Xpo1p, 0.2 μM FG-CFP-RanBD (Yrb2p), and 4.0 μM Gsp1p-GTP was rapidly mixed with either 4.0 μM Yrb2p (C), buffer alone, or 20 μM PKI (S35L) (F). (E) A solution of 0.2 μM YFP-Xpo1p, 0.2 μM CFP-FG-RanBD (Yrb2p), and 4.0 μM Gsp1p-GTP was rapidly mixed with either buffer alone, 20 μM PKI (S35L), or 4.0 μM Yrb2p.

(G) A diagram depicting the design of the chimeric mutant (YrbChimera) in which the C-terminal RanBD of Yrb2p is replaced with the RanBD of Yrb1p.

(H) GST pull-down assay. Immobilized GST-Gsp1p-GTP (30 μg) was incubated with Yrb1p (60 μg) or Yrb2p (60 μg) or YrbChimera (60 μg) with or without Xpo1p (60 μg).

(I) Stopped-flow traces. CFP was excited at 430 nm, and YFP emission was monitored. A solution of 0.2 μM Xpo1p-CFP and 3.0 μM Gsp1p-GTP was rapidly mixed with a solution of 1.0 μM YFP-NES and either buffer alone or 0.5 μM Yrb2p or 0.5 μM Yrb1p or 0.5 μM YrbChimera.

(Kuhlmann et al., 1997), are clearly weaker in the Yrb2p complex compared with the Yrb1p complex, and Gsp1p only weakly wraps around RanBD of Yrb2p. From the crystal structure of free RanBD of RanBP3 (Langer et al., 2011), it appears that Yrb2p and RanBP3 are similar in that the Gsp1p/Ran C terminus interacts with RanBD only very weakly (Supplemental Results and Discussion).

Moreover, the direct contacts made between Yrb1p RanBD and Xpo1p are entirely lost in Xpo1p-Yrb2p-Gsp1p-GTP complex (Figures 3A, 3B, and 3E–3G). The basic residues of Yrb1p (Lys88 and Lys130) that form salt bridges with the acidic residues of HEAT9 loop (Glu448 and Asp447, respectively) in Xpo1p-Yrb1p-Gsp1p-GTP complex are not conserved in Yrb2p, and so these salt bridges are not formed between Yrb2p and HEAT9 loop (Figures 3E and 3F). The direct contacts between RanBD and HEAT15, observed in the Yrb1p complex, are also lost in the Yrb2p complex due to changes in amino acid sequence and conformation of the β5–β6 loop of RanBD that form the interface with HEAT15 (Figure 3G). The loss of direct contacts between Xpo1p and RanBD is associated with movement of Xpo1p away from RanBD (indicated by an arrow in Figure 3G) and results in a small shift in the superhelical path of the C-terminal half of Xpo1p (Figure 3H). Thus, the structural data show that the RanBD contacts with both Gsp1p and Xpo1p are much less intimate in the Yrb2p complex and imply that the RanBD of Yrb2p would readily dissociate from the Xpo1p-Yrb2p-Gsp1p-GTP, in contrast to the RanBD of Yrb1p that binds strongly to Gsp1p-GTP and Xpo1p to displace NES. Indeed, pull-down assays showed that the binding of Xpo1p and Gsp1p to the RanBD of Yrb2p was hardly detectable (Figure 3I).

An Allosteric Mechanism of RanBD Displacement by NES Likely Underlies Rapid Binding of NES to Xpo1p-Yrb2p-Gsp1p-GTP Complex

In view of the fact that the association of RanBD is much less intimate in Xpo1p-Yrb2p-Gsp1p-GTP complex than in Xpo1p-Yrb1p-Gsp1p-GTP complex, two distinct models on the mechanism underlying the rapid NES binding to Xpo1p-Yrb2p-Gsp1p-GTP complex can be envisaged (Figures 4A and 4B).

One model is that NES binds to Xpo1p only after RanBD dissociates (a passive competition model; Figure 4A). If association of RanBD was extremely weak, the off-rate of RanBD would be high. Because Gsp1p-GTP is preloaded onto the inner surface of Xpo1p by Yrb2p, the dissociation of RanBD may be associated with movement of HEAT9 loop to Gsp1p and concomitant opening of the NES-binding cleft, which would enable stable binding of NES afterward. However, pull-down assays using deletion mutants of Yrb2p showed that the integrity of Xpo1p-Yrb2p-Gsp1p-GTP complex requires both FG-repeat domain and RanBD and that Gsp1p-GTP cannot form a stable complex with Xpo1p in the absence of RanBD (Figure 3I). Thus, once RanBD dissociates, the binding of Gsp1p to Xpo1p could become unstable immediately. This casts doubt on the passive competition model.

An alternative model (an active displacement model) is that NES displaces RanBD by an allosteric mechanism (Figure 4B). In other words, the reverse reaction of Yrb1p-induced displacement of NES may occur for Yrb2p. Our previous kinetic and structural data showed that Yrb1p binds Xpo1p-NES-Gsp1p-GTP complex to form a short-lived quaternary intermediate (Xpo1p-NES-Yrb1p-Gsp1p-GTP complex), which rapidly transforms into Xpo1p-Yrb1p-Gsp1p-GTP complex, releasing NES (Koyama and Matsuura, 2010). Crucial to this mechanism is that the binding of the RanBD of Yrb1p is strong enough to elicit the movement of HEAT9 loop (from Gsp1p to the concave side of the NES-binding cleft) and prevent its backward movement. This suggests that if the binding of RanBD were very weak (as is the case for Yrb2p and RanBP3) the reverse reaction (i.e., displacement of RanBD by NES through movement of HEAT9 loop toward Gsp1p/Ran) could occur easily, accounting for our kinetic data that NES binds rapidly to preformed Xpo1p-Yrb2p-Gsp1p-GTP complex. Although this active displacement mechanism necessitates the transient binding of NES to Xpo1p-Yrb2p-Gsp1p-GTP complex (before dissociation of RanBD) in the first place, recent structural studies indicate that this could indeed occur due to flexibility of Xpo1p. The crystal structures of Xpo1p in complex with Yrb1p, Gsp1p-GTP, and various CRM1 inhibitors (such as Leptomycin B) showed that the NES-binding cleft of Xpo1p-Yrb1p-Gsp1p-GTP complex is flexible enough to open at least partially to bind the small inhibitors even when HEAT9 loop adopts the autoinhibitory conformation (Sun et al., 2013). Thus, the conformational flexibility of Xpo1p could allow for weak binding of NES to Xpo1p-Yrb2p-Gsp1p-GTP complex without necessitating the movement of HEAT9 loop and dissociation of RanBD. The loss of direct contact between Xpo1p and the RanBD in Xpo1p-Yrb2p-Gsp1p-GTP complex indicates that the flexibility of Xpo1p in this complex may be enhanced compared with the Yrb1p complex and thus facilitates the transient binding of NES and subsequent conformational changes of Xpo1p (i.e., movement of HEAT9 loop and complete opening of the NES-binding cleft), leading to stable binding of NES and dissociation of the loosely bound RanBD.

Strong support for the active displacement model was obtained by examining the effect of NES on the off-rate of Yrb2p using FRET-based stopped-flow assays (Figures 4C–4F). As a control, we measured the off-rate of the RanBD of Yrb1p. As expected from the high affinity of Yrb1p RanBD, the rate of spontaneous dissociation of Yrb1p RanBD from Xpo1p and Gsp1p-GTP was slow (k_{off} = 0.80 s^{-1}; Figure 4C), and even a strong NES-cargo (PKI S35L mutant; Güttler et al., 2010) did not increase the off-rate of Yrb1p RanBD (Figure 4D). This suggests that the binding of Yrb1p RanBD is so strong that the reverse reaction of the active displacement of NES by Yrb1p RanBD is prevented effectively. In contrast, the NES-cargo increased the off-rate of Yrb2p (Figures 4C and 4F). To do this assay, we made three FRET constructs of CFP-Yrb2p fusion protein (CFP-FG-RanBD, in which CFP is fused to the N terminus of Yrb2p [residues 90–327]; FG-CFP-RanBD, in which CFP is inserted between residue 199 and 200 of Yrb2p [residues 90–327]; and Yrb2p-CFP, in which CFP is fused to the C terminus of Yrb2p). Unfortunately, the Yrb2p-CFP construct, which was expected to be the most suitable among the three constructs for FRET-based detection of the dissociation of RanBD, did not give detectable CFP-YFP FRET signal when incubated with YFP-Xpo1p and Gsp1p-GTP. Nevertheless, important supportive data were obtained using the other two FRET constructs in stopped-flow experiments. Rapid mixing of a preincubated mixture (YFP-Xpo1p, Gsp1p, and CFP-FG-RanBD) with a large excess of unlabeled Yrb2p gave k_{off} of 0.319 s^{-1} (Figure 4E), and this off-rate was not increased by PKI (S35L) (Figure 4E). Because CFP is tethered to the N terminus of FG repeats in the CFP-FG-RanBD construct, the decrease in the FRET signal would be sensitive to dissociation of FG repeats, and the kinetic data indicate that NES does not increase the rather slow off-rate of FG repeats. In contrast, a much faster rate of spontaneous dissociation (k_{off} = 1.24 s^{-1}) was observed when FG-CFP-RanBD was used (Figure 4C). Because CFP is inserted immediately before RanBD in FG-CFP-RanBD, this construct would be far more sensitive to the dissociation of RanBD than the CFP-FG-RanBD construct, and so the kinetic data indicate that the rate of spontaneous dissociation of RanBD is much faster than that of the FG repeats of Yrb2p. Importantly, the PKI (S35L) dramatically increased the off-rate measured by using FG-CFP-RanBD by 11-fold (k_{off} = 13.3 s^{-1}), supporting the idea that NES actively displaces RanBD of Yrb2p from the Xpo1p-Yrb2p-Gsp1p-GTP complex (Figure 4F). Taken together, the structural and biochemical data suggest that the active displacement mechanism underlies the rapid NES-binding to Xpo1p-Yrb2p-Gsp1p-GTP complex.

To further verify the functional importance of the RanBD's affinity for Gsp1p-GTP, we used a chimeric mutant of Yrb2p (referred to as YrbChimera; Taura et al., 1997) in which the weak-binding RanBD of Yrb2p is replaced with the RanBD of Yrb1p that binds Gsp1p-GTP much more strongly (Figures 4G and 4H). YrbChimera did not retain the Yrb2p's ability to accelerate NES association in the presence of Gsp1p-GTP and instead inhibited the NES binding like Yrb1p (Figure 4I). Thus, it is important that Yrb2p has only extremely low affinity for Gsp1p-GTP in order to allow for rapid binding of cargo to Xpo1p-Yrb2p-Gsp1p-GTP complex. These results are consistent with the previous in vivo functional analyses, in which the same chimeric mutant of Yrb2p did not rescue the cold sensitivity of *yrb2*Δ yeast cells

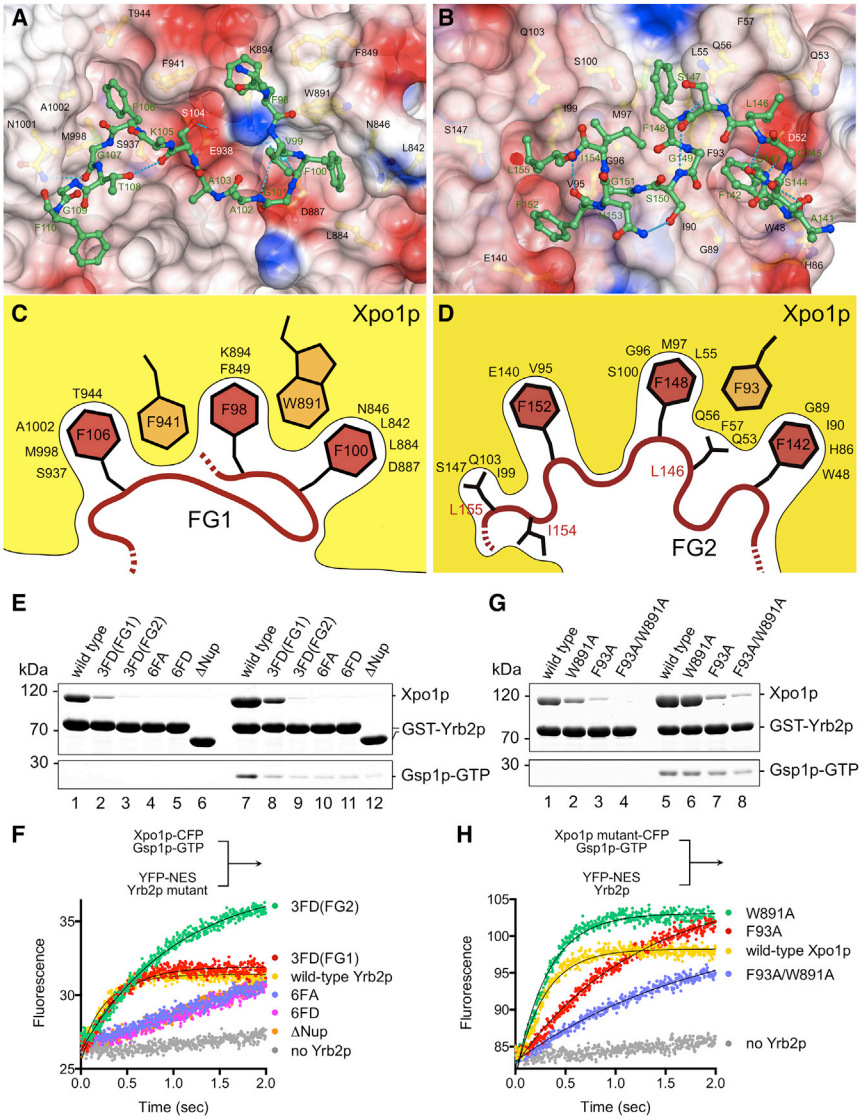

Figure 5. Recognition of the FG-Repeats of Yrb2p by Xpo1p and In Vitro Mutational Analyses

(A and B) Interactions involving FG1 (A) or FG2 (B) with key residues shown under the transparent surface (colored by electrostatic potential: blue, positive; red, negative; white, neutral) of Xpo1p.

(C and D) Schematic diagram of recognition of the FG repeats by Xpo1p.

(E and F) Mutational analyses of the FG-repeats of Yrb2p.

(G and H) Mutational analyses of the FG-repeat binding sites of Xpo1p.

In GST pull-down assays (E and G), immobilized GST-Yrb2p (25 μg) was incubated with Xpo1p (50 μg) with (lanes 7–12 in E and lanes 5–8 in G) or without (lanes 1–6 in E and lanes 1–4 in G) Gsp1p-GTP (50 μg). In stopped-flow assays (F and H), a solution of 0.2 μM Xpo1p-CFP and 3.0 μM Gsp1p-GTP was rapidly mixed with a solution of 1.0 μM YFP-NES and either buffer alone or 0.5 μM Yrb2p. CFP was excited at 430 nm, and YFP emission was monitored. ΔNup refers to a Yrb2p mutant in which the entire FG-repeat domain (residues 94–149) is deleted (Taura et al., 1998). See also Figure S4.

and was toxic for cell growth when overexpressed (Taura et al., 1997).

Specific Recognition of Yrb2p FG Repeats by Xpo1p

At each of the FG-repeat binding sites identified in the structure of Xpo1p-Yrb2p-Gsp1p-GTP complex, three phenylalanine side chains of Yrb2p (Phe98, Phe100, and Phe106 in FG1; Phe142, Phe148, and Phe152 in FG2) were buried in hydrophobic depressions between adjacent HEAT repeats on the convex surface of Xpo1p (Figures 5A–5D). This is reminiscent of the way FG-nups bind to importin β (Bayliss et al., 2000; Liu and Stewart, 2005) and suggests that importin-β-like NTRs commonly have the FG-repeat binding sites on their outer face. At each site, the binding pockets for the phenylalanine side chains of Yrb2p are defined by a number of aliphatic and aromatic residues of Xpo1p (Figures 5A–5D; see also Figures S4A and S4B for details). Thus, phenylalanine side chains of FG repeats are recognized through a combination of hydrophobic and aromatic (π-π) interactions. Furthermore, Yrb2p residues adjacent to the key phenylalanine residues in FG1 and FG2 made intimate contacts with Xpo1p via multiple hydrogen bonds and van der Waals contacts, conferring stability and specificity in Yrb2p-Xpo1p binding (Figures S4A and S4B). These intimate contacts were associated with the main chain of Yrb2p making sharp turns immediately following or preceding the key Phe residues, and the Gly residues in both FG1 and FG2 enabled Yrb2p to adopt these conformations. More details of the recognition of FG-repeats are described in the Supplemental Results and Discussion (Figure S4).

Mutational Analyses of the Interactions between Xpo1p and Yrb2p FG Repeats

We used structure-based mutants of Yrb2p and Xpo1p to verify that the interactions between Xpo1p and FG repeats of Yrb2p are important for Yrb2p's function to accelerate export complex assembly (Figures 5E–5H). In pull-down assays, substitution of three phenylalanines of FG1 with aspartic acids (3FD [FG1] mutant) reduced the binding of Xpo1p to Yrb2p both in the presence and absence of Gsp1p-GTP, and substitution of three phenylalanines of FG2 with aspartic acids (3FD [FG2] mutant) was more effective in reducing Xpo1p binding (Figure 5E). Substitution of all six phenylalanines of the FG-repeat domain with alanines (6FA mutant) or aspartic acids (6FD mutant) decreased the Xpo1p binding to an undetectable level (Figure 5E). Consistently, in stopped-flow experiments, the 3FD (FG2) mutations

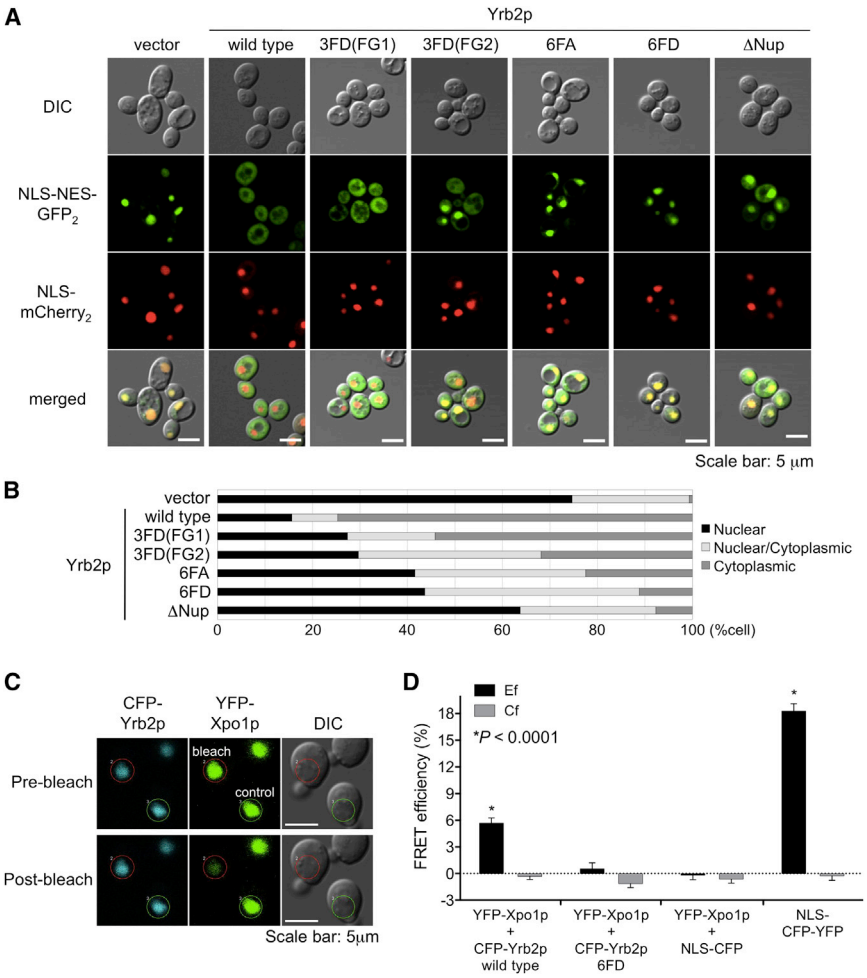

Figure 6. Yeast In Vivo Functional Analyses of the Interactions between FG Repeats and Xpo1p

(A and B) In vivo nuclear transport assays. NLS-NES-GFP_2 was expressed in *S. cerevisiae yrb2Δ* cells that express plasmid-encoded WT Yrb2p or its derivatives, and the subcellular localization of NLS-NES-GFP_2 was analyzed. NLS-$mCherry_2$ was coexpressed to identify the nucleus. (A) Representative images of the cells. DIC, differential interference contrast. The scale bar represents 5 μm. (B) Localization of NLS-NES-GFP_2 was scored in 150 to 200 cells as Nuclear (black), Nuclear/Cytoplasmic (comparable intensity in the nucleus and the cytoplasm; light gray), or Cytoplasmic (dark gray).

(C and D) In vivo CFP-YFP FRET imaging (evaluated by acceptor photobleaching) detected Xpo1p-Yrb2p interactions in the nucleus. (C) Representative images of the yeast cells expressing YFP-Xpo1p and CFP-Yrb2p before and after photobleaching of YFP are shown. Bleached ROI is represented by red circle, and the control (nonbleached) ROI by green circle. The scale bar represents 5 μm. (D) FRET energy transfer efficiencies in the bleached ROIs (E_f) and in the control ROIs (C_f) were calculated for each strain, and average values are shown. Error bars represent SE, n = 10. *p < 0.0001 by two-tailed Student's t test.

See also Figure S5.

decreased the rate of NES association to Xpo1p in the presence of Gsp1p-GTP by a factor of 3, and although the 3FD (FG1) mutations decreased the on-rate of NES only slightly, they exacerbated the effect of 3FD (FG2) mutations (Figure 5F; Table S1). Mutations on Xpo1p's side were also effective. Substitution of $Trp891^{Xpo1p}$ (that contacts two of the key phenylalanines of FG1; Figures 5A and 5C) with alanine reduced Xpo1p binding to Yrb2p, and substitution of $Phe93^{Xpo1p}$ (that contacts two of the key phenylalanines and also Leu146 of FG2; Figures 5B and 5D) with alanine more effectively reduced Xpo1p binding (Figure 5G). Likewise, F93A mutation was more effective than W891A mutation in decreasing the rate of NES association to Xpo1p in the presence of Gsp1p-GTP and Yrb2p, and when combined, W891A mutation exacerbated the effect of F93A mutation (Figure 5H; Table S1). Taken together, our data demonstrate that both FG1 and FG2 contribute to Yrb2p's activity to accelerate NES binding in vitro.

Do the interactions between FG-repeats and Xpo1p observed in the crystal structure of Xpo1p-Yrb2p-Gsp1p-GTP complex contribute to NES-protein export in vivo? To address this question, we expressed fluorescent reporter protein (NLS-NES-GFP_2) in yeast cells and examined the effect of Yrb2p mutations on the subcellular localization of the reporter protein. In agreement with previous studies (Taura et al., 1998; Noguchi et al., 1999), the efficiency of nuclear export of this reporter protein is decreased substantially in *yrb2Δ* cells, and expression of WT Yrb2p restored efficient export (Figures 6A and 6B). However, the 3FD (FG1) or 3FD (FG2) mutant of Yrb2p was not as effective as WT Yrb2p in restoring nuclear export, and more drastic mutations (6FA or 6FD mutations) were even less effective in restoring export activity (Figures 6A and 6B). These data demonstrate that both the Xpo1p-FG1 and Xpo1p-FG2 interactions observed in the crystal structure are important for efficient Xpo1p-mediated export in vivo.

We also used the 6FD mutant to demonstrate that the FG repeats of Yrb2p binds to Xpo1p in the nucleus by FRET imaging of living yeast cells in which fluorescent fusion proteins (YFP-Xpo1p and CFP-Yrb2p [NLS-CFP-FG-RanBD]) are expressed in place of WT proteins (Figures 6C and 6D). YFP-Xpo1p complemented WT Xpo1p in yeast cells, and CFP-Yrb2p rescued the cold sensitivity of *yrb2Δ* cells, demonstrating that both YFP-Xpo1p and CFP-Yrb2p are functional in vivo (Figure S5). We employed the acceptor photobleaching technique to detect CFP-YFP FRET signal (Karpova et al., 2003; Figures 6C and 6D). A positive control (NLS-CFP-YFP fusion protein) showed conspicuous FRET signal in the nucleus (Figure 6D). When YFP-Xpo1p and CFP-Yrb2p were coexpressed in yeast cells, both proteins localized primarily in the nucleus (Figure 6C), and the CFP-YFP FRET signal was indeed detected in the nucleus

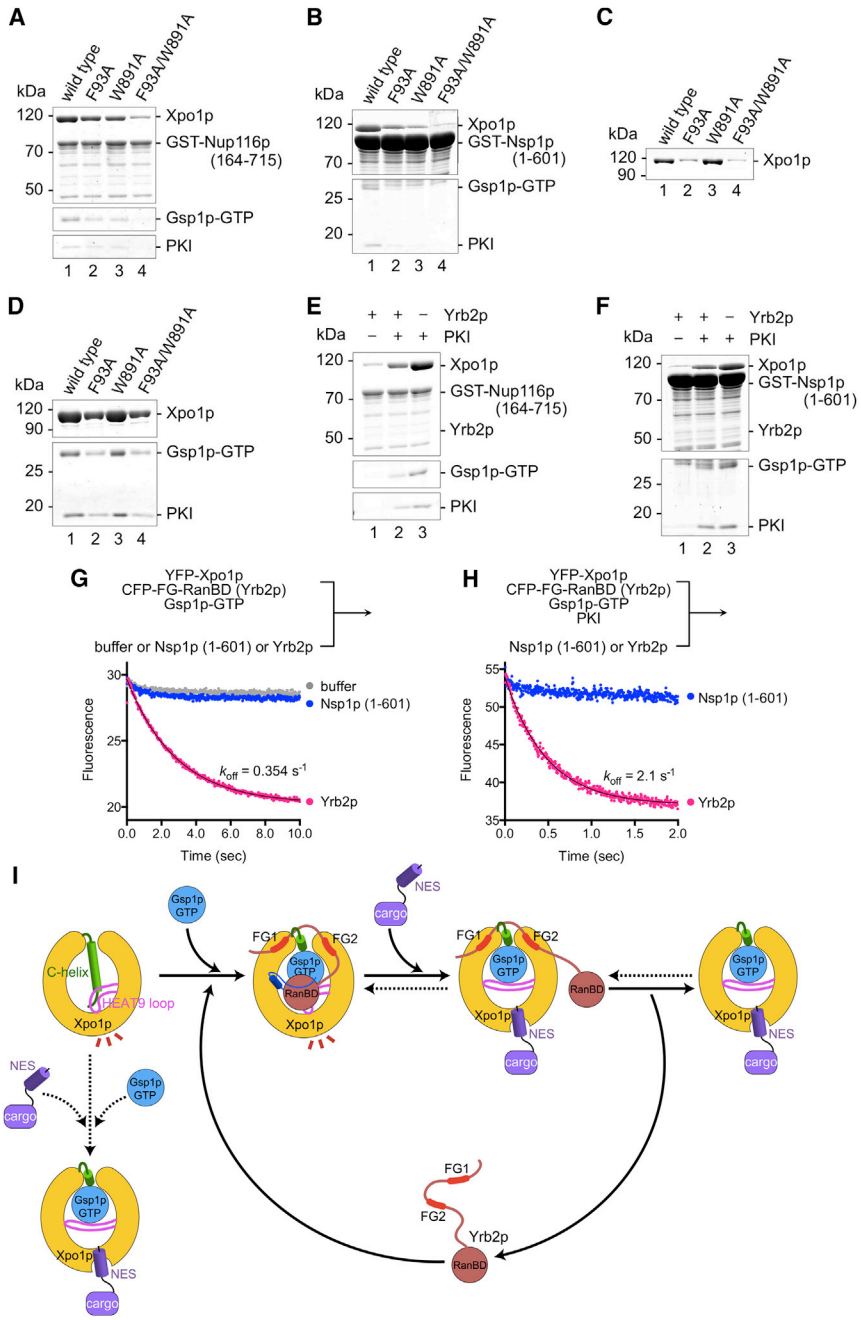

Figure 7. Functional Analyses of the Interactions between FG-Nups and Xpo1p and Proposed Mechanism of Yrb2p Action

(A–F) Pull-down assays. In (A) and (B), immobilized GST-Nup116p (residues 164–715) (19 μg) or GST-Nsp1p (residues 1–601) (107 μg) was incubated with Xpo1p (WT [lane 1] or mutants [lanes 2–4]) (30 μg), Gsp1p-GTP (40 μg), and PKI (S35L) (50 μg). In (C) and (D), phenyl-sepharose beads were incubated with Xpo1p (WT [lane 1] or mutants [lanes 2–4]) (30 μg) with (D) or without (C) Gsp1p-GTP (40 μg) and PKI (50 μg). In (E) and (F), immobilized GST-Nup116p (residues 164–715) (19 μg) or GST-Nsp1p (residues 1–601) (107 μg) was incubated with Xpo1p (30 μg) and Gsp1p-GTP (50 μg) with or without Yrb2p (50 μg in E and 10 μg in F) and PKI (S35L) (1.0 mg).

(G and H) Stopped-flow traces. In (G), a solution of 0.2 μM YFP-Xpo1p, 0.2 μM CFP-FG-RanBD (Yrb2p) and 4.0 μM Gsp1p-GTP was rapidly mixed with buffer or 4.0 μM Nsp1p (residues 1–601) or 4.0 μM Yrb2p. In (H), a solution of 0.2 μM YFP-Xpo1p, 0.2 μM CFP-FG-RanBD (Yrb2p), 4.0 μM Gsp1p-GTP, and 20 μM PKI (S35L) was rapidly mixed with 20 μM Nsp1p (residues 1–601) or 4.0 μM Yrb2p.

(I) A model for how Yrb2p facilitates the initial step of the Xpo1p-mediated nuclear export. The spontaneous assembly of Xpo1p-cargo-Gsp1p-GTP complex is slow, whereas Yrb2p-assisted assembly of the export complex is much faster. See the text for details.

See also Figure S6.

for WT proteins but was not detected when 6FD mutations were introduced to CFP-Yrb2p (Figure 6D). As a negative control, co-expression of NLS-CFP and YFP-Xpo1p did not yield detectable CFP-YFP FRET signal in the nucleus (Figure 6D). Thus, the FRET imaging provided direct evidence that FG repeats of Yrb2p binds to Xpo1p in the nucleus in living yeast cells.

Yrb2p and FG Nucleoporins Compete for the Same Sites on Xpo1p

The structure-based mutants also provided evidence that the FG-repeat binding sites observed in the crystal structure of Xpo1p-Yrb2p-Gsp1p-GTP complex also serve as binding sites for FG-nups (Figures 7A and 7B). We used GLFG-repeat domain of *S. cerevisiae* Nup116p (residues 164–715) and FG/FxFG-repeat domain of *S. cerevisiae* Nsp1p (residues 1–601) for the binding assays. These two types of FG-nups are localized in the central channel of yeast NPCs (Rout et al., 2000) and are likely important to maintain the permeability barrier of NPCs and at the same time allow selective passage of NTRs through interactions between NTRs and the FG-repeat motifs (Hülsmann et al., 2012). Mutations of aromatic residues of Xpo1p in the FG1 and FG2 binding sites (F93A and W891A), particularly when combined, dramatically reduced the binding of Xpo1p to Nup116p and Nsp1p in the presence of Gsp1p-GTP and PKI in pull-down assays, suggesting that these sites are the major binding sites for both types of FG-nups (Figures 7A and 7B).

However, the above results do not necessarily preclude the possibility that there are residual binding sites (other than the FG1 and FG2 binding sites) for FG-nups on Xpo1p. In general, importin-β-like NTRs have many binding sites for FG repeats on their outer surface, and the interactions between the NTRs and

FG repeats are rather weak and have high off-rates (Stewart et al., 2001; Stewart, 2007). These weak interactions are hard to detect by pull-down assays using immobilized GST-nups because the beads have to be washed for analysis. Even when Yrb2p is bound to Xpo1p, most of the outer surface of Xpo1p is still exposed to solvent and may contain a number of weak and high-off-rate binding sites for FG-nups. To test this possibility, we used phenyl-sepharose resin, which is a rather strong mimic of FG domains and is suitable to detect weak binding of NTRs to FG repeats (Ribbeck and Görlich, 2002). Although the double mutations (F93A/W891A) of Xpo1p at the FG1 and FG2 binding sites weakened the binding of Xpo1p alone or Xpo1p-PKI-Gsp1p-GTP complex to phenyl-sepharose, a substantial amount of the double mutant bound to phenyl-sepharose, particularly in the presence of PKI and Gsp1p-GTP (Figures 7C and 7D). Thus, the binding sites for the FG repeats of Yrb2p may not be the only binding sites for FG-nups. Similar consideration may also hold true for RanBP3 because previous studies using digitonin-permeabilized cells showed that RanBP3 inhibits the binding of CRM1 to NPCs to some extent and that RanBP3 binds to NPCs in a CRM1- and Ran-dependent manner (Lindsay et al., 2001).

The above mutational analyses indicate that Yrb2p and FG-nups compete for the same sites (FG1 and FG2 binding sites) on Xpo1p, although there may be additional low-affinity binding sites for FG repeats of nups. Consistently, although the binding of Xpo1p-PKI-Gsp1p-GTP complex to Nup116p and Nsp1p was readily detectable by a pull-down assay, the binding of Xpo1p to these FG-nups was weak (but still detectable) when Yrb2p was added together with Gsp1p-GTP to Xpo1p (Figures 7E and 7F). Remarkably, the addition of PKI to Xpo1p, Yrb2p, and Gsp1p-GTP restored the binding of Xpo1p (together with Gsp1p-GTP and PKI, but not together with Yrb2p) to Nup116p and Nsp1p to some extent (lane 2 of Figures 7E and 7F). Similar results were obtained when human RanBP3, CRM1, and Ran were used instead of yeast Yrb2p, Xpo1p, and Gsp1p, respectively (Figures S6A and S6B). These data suggest that the binding of the NES-cargo to the assembly intermediate (Xpo1p-Yrb2p-Gsp1p-GTP complex or CRM1-RanBP3-Ran-GTP complex) promotes dissociation of Yrb2p (RanBP3) and in turn promotes association of FG-nups to Xpo1p (CRM1).

In principle, the competition between Yrb2p and FG-nups for the same sites on Xpo1p could be either passive or active, and these two possibilities can be distinguished by investigating the effect of FG-nups on the off-rate of Yrb2p. In the passive competition mechanism, FG-nups can bind to the FG1 and FG2 binding sites only after Yrb2p has spontaneously dissociated from Xpo1p. In this case, FG-nups do not increase the off-rate of Yrb2p. In the active competition mechanism, FG-nups induce dissociation of Yrb2p and thereby increase the off-rate of Yrb2p. We therefore measured the off-rate of Yrb2p using a FRET-based stopped-flow assay (Figures 7G and 7H). We used the CFP-FG-RanBD construct of Yrb2p in this assay because this is suitable for FRET-based detection of dissociation of Yrb2p FG-repeats. Importantly, Nsp1p did not increase the off-rate of Yrb2p both in the presence and absence of PKI (S35L) (Figures 7G and 7H). These results suggest that the competition between Yrb2p and FG-nups for the binding to the same sites on Xpo1p is passive. This is not in conflict with the results of pull-down assays (lane 1 of Figures 7E and 7F) because the immobilized FG-nups were incubated with Yrb2p, Xpo1p, and Gsp1p-GTP in the pull-down assays for as long as 1 hour, which would be long enough for replacement of FG-nups with Yrb2p even if the competition to bind the same sites on Xpo1p is passive and thus is slow and is not evident in the time scale (on the order of seconds) of the stopped-flow experiments (Figures 7G and 7H).

An Assisted-Assembly Model of the Xpo1p Nuclear Export Complex

On the basis of all of the structural and functional evidence described above, we propose a mechanism of action of Yrb2p in Xpo1p-mediated nuclear export (Figure 7I).

The FG repeats and RanBD of Yrb2p would first recruit Gsp1p-GTP to Xpo1p to form a ternary Xpo1p-Yrb2p-Gsp1p-GTP complex. Because of the high specificity in Yrb2p binding to Xpo1p, Yrb2p is involved in the Xpo1p export pathway but leaves other nuclear export pathways unaffected. The overall structure of the assembly intermediate (Xpo1p-Yrb2p-Gsp1p-GTP complex) reported here is similar to the previously determined structure of the disassembly intermediate in the cytoplasm (Xpo1p-Yrb1p-Gsp1p-GTP complex; Koyama and Matsuura, 2010) and the NES-binding cleft is closed in both complexes. However, unlike Yrb1p, the weak binding nature of Yrb2p RanBD enables NES to displace RanBD easily. Thus, Yrb2p accelerates the association of both Gsp1p-GTP and cargo to Xpo1p. Yrb2p does not bind directly to cargo but instead exploits allostery in Xpo1p to mediate rapid loading of cargo.

In our model, the NES binding causes at least partial dissociation of Yrb2p (i.e., dissociation of RanBD) but does not require complete dissociation of Yrb2p, and Yrb2p FG repeats can stay bound on Xpo1p after cargo loading. The dissociation of Yrb2p FG-repeats from Xpo1p relies on spontaneous dissociation and is rather slow. The complete dissociation of Yrb2p from the export complex could occur in the nucleus. In this case, the dissociated Yrb2p would immediately participate in another round of rapid assembly of the Xpo1p nuclear export complex in the nucleus. However, our data indicate that it is also possible that Yrb2p accompanies the Xpo1p-cargo-Gsp1p-GTP complex to translocate across the NPC, as suggested previously for RanBP3 (Lindsay et al., 2001). There are three reasons why this may occur. First, the FG1 and FG2 binding sites observed in the crystal structure of Xpo1p-Yrb2p-Gsp1p-GTP complex may not be the only binding sites for FG-repeat motifs, and the residual binding sites could be sufficient to mediate NPC passage. Second, it appears that FG-nups do not accelerate dissociation of Yrb2p and compete with Yrb2p only passively to bind to the same FG-binding sites on Xpo1p, and so Yrb2p can probably stay bound to Xpo1p even in the central channel of the NPC (where the local concentration of FG repeats is extremely high) until Yrb2p dissociates spontaneously. Finally, the rate of spontaneous dissociation of Yrb2p from Xpo1p and Gsp1p-GTP even in the presence of the NES-cargo is not very high (k_{off} = 2.1 s^{-1}; $t_{1/2}$ = 0.33 s; Figure 7H). It is therefore conceivable that Yrb2p can remain bound to Xpo1p during the time scale of NPC passage of the nuclear export complex, provided that the NPC passage time of nuclear export is similar to that of nuclear import, which can be as short as 10 ms for cargoes containing classical NLSs, as

reported by a single molecule study (Yang et al., 2004). Thus, we propose that dissociation of Yrb2p may occur before, during, or after the NPC passage of the Xpo1p nuclear export complex. These possibilities are not mutually exclusive to each other.

In summary, we discovered the function of Yrb2p (RanBP3) to increase the rate of assembly of the Xpo1p (CRM1) nuclear export complex. The crystal structure of Xpo1p-Yrb2p-Gsp1p-GTP complex provided a structural rationale to understand how FG repeats and RanBD of Yrb2p mediate rapid association of Gsp1p-GTP and the NES-cargo to Xpo1p. The model we propose is fully supported by mutational analyses, which also provided insights into how FG-nups interact with Xpo1p. This study also extends our previous study (Koyama and Matsuura, 2010) by providing a general implication that the same framework of active displacement mechanism (i.e., RanBD and NES displace each other through allosteric conformational changes of Xpo1p) underlies both Yrb1p-mediated rapid disassembly of export complex in the cytoplasm and also Yrb2p-mediated rapid assembly of export complex in the nucleus.

EXPERIMENTAL PROCEDURES

A detailed description of the methods employed in this study is provided in the Supplemental Experimental Procedures.

Protein Preparation

Recombinant proteins were expressed in *E. coli* and purified for biochemical assays and crystallization.

Crystallography

Crystals of Xpo1p-Yrb2p-Gsp1p-GTP complex and crystals of Xpo1p-PKI-Gsp1p-GTP complex were grown at 20°C by hanging drop vapor diffusion. Diffraction data were collected from cryoprotected crystals at SPring-8. The structures were determined by molecular replacement using Xpo1p-Yrb1p-Gsp1p-GTP complex (PDB code, 3M1I; Koyama and Matsuura, 2010) as a search model. A comment on unexplained density (Figure S7) is provided in the Supplemental Experimental Procedures.

Biochemistry

Association and dissociation kinetics were measured at 20°C using a Hi-Tech Scientific SF-61DX2 stopped-flow spectrophotometer, except that slow kinetics was measured by manual mixing using a JASCO FP-6500 spectrofluorometer. Time-dependent increase or decrease of CFP-YFP FRET signal was analyzed by nonlinear regression using GraphPad Prism to determine the association and dissociation rates. Pull-down assays were performed as described (Matsuura and Stewart, 2004). Circular dichroism spectra were recorded at 20°C with a JASCO J-720WN spectrophotometer.

Cell Biology

To analyze nuclear transport, NLS-NES-GFP_2 was expressed in yeast cells, and GFP signals were monitored. For FRET imaging in vivo, yeast cells expressing YFP-Xpo1p and CFP-Yrb2p were examined using an Olympus FV1000 confocal microscope, and CFP-YFP FRET signals were analyzed by acceptor photobleaching technique (Karpova et al., 2003). The area to be bleached was defined by drawing a region of interest (ROI) that was set to contain the entire nucleus of the cell. FRET energy transfer efficiencies of the bleached ROIs (E_f) and control nonbleached ROIs (C_f) were calculated using the formula

$$E_f(C_f) = (I_a - I_b) \times 100/I_a,$$

where I_b and I_a are the CFP intensities just before and after the bleach, respectively.

ACCESSION NUMBERS

Atomic coordinates and structure factors for the reported crystal structures have been deposited in the Protein Data Bank (http://www.rcsb.org) under accession codes 3WYF (Xpo1p-Yrb2p-Gsp1p-GTP complex) and 3WYG (Xpo1p-PKI-Gsp1p-GTP complex).

SUPPLEMENTAL INFORMATION

Supplemental Information includes Supplemental Experimental Procedures, seven figures, and four tables and can be found with this article online at http://dx.doi.org/10.1016/j.celrep.2014.09.052.

AUTHOR CONTRIBUTIONS

M.K. and Y.M. conceived the project. M.K. performed the majority of the experiments, with the contribution of N.S. and under the supervision of Y.M. M.K. and Y.M. wrote the manuscript.

ACKNOWLEDGMENTS

We thank Hirofumi Onishi, Yoshikatsu Sato, Natsumi Saito, Junya Kobayashi, and Hidemi Hirano for assistance and discussion and Photon Factory and SPring-8 staff for assistance during data collection. The data collection at Photon Factory was performed with the approval of the Photon Factory Program Advisory Committee (proposal nos. 2009G136 and 2011G585). The data collection at SPring-8 was performed with the approval of the Japan Synchrotron Radiation Research Institute (JASRI) (proposal nos. 2011A1093, 2011B1083, 2012B1291, and 2013B1129). This work was supported by the Sumitomo Foundation and JSPS/MEXT KAKENHI (18687010, 21770109, 23770110, 25121713, 10J05907, and 24030003). M.K. was supported by JSPS Research Fellowship.

Received: July 31, 2013
Revised: January 25, 2014
Accepted: September 28, 2014
Published: October 30, 2014

REFERENCES

Bayliss, R., Littlewood, T., and Stewart, M. (2000). Structural basis for the interaction between FxFG nucleoporin repeats and importin-beta in nuclear trafficking. Cell *102*, 99–108.

Chari, A., and Fischer, U. (2010). Cellular strategies for the assembly of molecular machines. Trends Biochem. Sci. *35*, 676–683.

Cronshaw, J.M., Krutchinsky, A.N., Zhang, W., Chait, B.T., and Matunis, M.J. (2002). Proteomic analysis of the mammalian nuclear pore complex. J. Cell Biol. *158*, 915–927.

Denning, D.P., Patel, S.S., Uversky, V., Fink, A.L., and Rexach, M. (2003). Disorder in the nuclear pore complex: the FG repeat regions of nucleoporins are natively unfolded. Proc. Natl. Acad. Sci. USA *100*, 2450–2455.

Dingwall, C., Kandels-Lewis, S., and Séraphin, B. (1995). A family of Ran binding proteins that includes nucleoporins. Proc. Natl. Acad. Sci. USA *92*, 7525–7529.

Dölker, N., Blanchet, C.E., Voß, B., Haselbach, D., Kappel, C., Monecke, T., Svergun, D.I., Stark, H., Ficner, R., Zachariae, U., et al. (2013). Structural determinants and mechanism of mammalian CRM1 allostery. Structure *21*, 1350–1360.

Dong, X., Biswas, A., Süel, K.E., Jackson, L.K., Martinez, R., Gu, H., and Chook, Y.M. (2009). Structural basis for leucine-rich nuclear export signal recognition by CRM1. Nature *458*, 1136–1141.

Ellis, R.J. (2001). Macromolecular crowding: obvious but underappreciated. Trends Biochem. Sci. *26*, 597–604.

Ellis, R.J. (2006). Molecular chaperones: assisting assembly in addition to folding. Trends Biochem. Sci. *31*, 395–401.

Englmeier, L., Fornerod, M., Bischoff, F.R., Petosa, C., Mattaj, I.W., and Kutay, U. (2001). RanBP3 influences interactions between CRM1 and its nuclear protein export substrates. EMBO Rep. *2*, 926–932.

Fornerod, M., Ohno, M., Yoshida, M., and Mattaj, I.W. (1997). CRM1 is an export receptor for leucine-rich nuclear export signals. Cell *90*, 1051–1060.

Frey, S., and Görlich, D. (2007). A saturated FG-repeat hydrogel can reproduce the permeability properties of nuclear pore complexes. Cell *130*, 512–523.

Fukuda, M., Asano, S., Nakamura, T., Adachi, M., Yoshida, M., Yanagida, M., and Nishida, E. (1997). CRM1 is responsible for intracellular transport mediated by the nuclear export signal. Nature *390*, 308–311.

Görlich, D., and Kutay, U. (1999). Transport between the cell nucleus and the cytoplasm. Annu. Rev. Cell Dev. Biol. *15*, 607–660.

Güttler, T., Madl, T., Neumann, P., Deichsel, D., Corsini, L., Monecke, T., Ficner, R., Sattler, M., and Görlich, D. (2010). NES consensus redefined by structures of PKI-type and Rev-type nuclear export signals bound to CRM1. Nat. Struct. Mol. Biol. *17*, 1367–1376.

Hülsmann, B.B., Labokha, A.A., and Görlich, D. (2012). The permeability of reconstituted nuclear pores provides direct evidence for the selective phase model. Cell *150*, 738–751.

Karpova, T.S., Baumann, C.T., He, L., Wu, X., Grammer, A., Lipsky, P., Hager, G.L., and McNally, J.G. (2003). Fluorescence resonance energy transfer from cyan to yellow fluorescent protein detected by acceptor photobleaching using confocal microscopy and a single laser. J. Microsc. *209*, 56–70.

Kehlenbach, R.H., Assheuer, R., Kehlenbach, A., Becker, J., and Gerace, L. (2001). Stimulation of nuclear export and inhibition of nuclear import by a Ran mutant deficient in binding to Ran-binding protein 1. J. Biol. Chem. *276*, 14524–14531.

Koyama, M., and Matsuura, Y. (2010). An allosteric mechanism to displace nuclear export cargo from CRM1 and RanGTP by RanBP1. EMBO J. *29*, 2002–2013.

Kuhlmann, J., Macara, I., and Wittinghofer, A. (1997). Dynamic and equilibrium studies on the interaction of Ran with its effector, RanBP1. Biochemistry *36*, 12027–12035.

Langer, K., Dian, C., Rybin, V., Müller, C.W., and Petosa, C. (2011). Insights into the function of the CRM1 cofactor RanBP3 from the structure of its Ran-binding domain. PLoS ONE *6*, e17011.

Lindsay, M.E., Holaska, J.M., Welch, K., Paschal, B.M., and Macara, I.G. (2001). Ran-binding protein 3 is a cofactor for Crm1-mediated nuclear protein export. J. Cell Biol. *153*, 1391–1402.

Liu, S.M., and Stewart, M. (2005). Structural basis for the high-affinity binding of nucleoporin Nup1p to the Saccharomyces cerevisiae importin-beta homologue, Kap95p. J. Mol. Biol. *349*, 515–525.

Matsuura, Y., and Stewart, M. (2004). Structural basis for the assembly of a nuclear export complex. Nature *432*, 872–877.

Mohr, D., Frey, S., Fischer, T., Güttler, T., and Görlich, D. (2009). Characterisation of the passive permeability barrier of nuclear pore complexes. EMBO J. *28*, 2541–2553.

Monecke, T., Güttler, T., Neumann, P., Dickmanns, A., Görlich, D., and Ficner, R. (2009). Crystal structure of the nuclear export receptor CRM1 in complex with Snurportin1 and RanGTP. Science *324*, 1087–1091.

Monecke, T., Haselbach, D., Voß, B., Russek, A., Neumann, P., Thomson, E., Hurt, E., Zachariae, U., Stark, H., Grubmüller, H., et al. (2013). Structural basis for cooperativity of CRM1 export complex formation. Proc. Natl. Acad. Sci. USA *110*, 960–965.

Nachury, M.V., and Weis, K. (1999). The direction of transport through the nuclear pore can be inverted. Proc. Natl. Acad. Sci. USA *96*, 9622–9627.

Noguchi, E., Hayashi, N., Nakashima, N., and Nishimoto, T. (1997). Yrb2p, a Nup2p-related yeast protein, has a functional overlap with Rna1p, a yeast Ran-GTPase-activating protein. Mol. Cell. Biol. *17*, 2235–2246.

Noguchi, E., Saitoh, Yh., Sazer, S., and Nishimoto, T. (1999). Disruption of the YRB2 gene retards nuclear protein export, causing a profound mitotic delay, and can be rescued by overexpression of XPO1/CRM1. J. Biochem. *125*, 574–585.

Ossareh-Nazari, B., Bachelerie, F., and Dargemont, C. (1997). Evidence for a role of CRM1 in signal-mediated nuclear protein export. Science *278*, 141–144.

Patel, S.S., Belmont, B.J., Sante, J.M., and Rexach, M.F. (2007). Natively unfolded nucleoporins gate protein diffusion across the nuclear pore complex. Cell *129*, 83–96.

Ribbeck, K., and Görlich, D. (2002). The permeability barrier of nuclear pore complexes appears to operate via hydrophobic exclusion. EMBO J. *21*, 2664–2671.

Rout, M.P., Aitchison, J.D., Suprapto, A., Hjertaas, K., Zhao, Y., and Chait, B.T. (2000). The yeast nuclear pore complex: composition, architecture, and transport mechanism. J. Cell Biol. *148*, 635–651.

Sabri, N., Roth, P., Xylourgidis, N., Sadeghifar, F., Adler, J., and Samakovlis, C. (2007). Distinct functions of the Drosophila Nup153 and Nup214 FG domains in nuclear protein transport. J. Cell Biol. *178*, 557–565.

Saito, N., and Matsuura, Y. (2013). A 2.1-Å-resolution crystal structure of unliganded CRM1 reveals the mechanism of autoinhibition. J. Mol. Biol. *425*, 350–364.

Stade, K., Ford, C.S., Guthrie, C., and Weis, K. (1997). Exportin 1 (Crm1p) is an essential nuclear export factor. Cell *90*, 1041–1050.

Stewart, M. (2007). Molecular mechanism of the nuclear protein import cycle. Nat. Rev. Mol. Cell Biol. *8*, 195–208.

Stewart, M., Baker, R.P., Bayliss, R., Clayton, L., Grant, R.P., Littlewood, T., and Matsuura, Y. (2001). Molecular mechanism of translocation through nuclear pore complexes during nuclear protein import. FEBS Lett. *498*, 145–149.

Strawn, L.A., Shen, T., Shulga, N., Goldfarb, D.S., and Wente, S.R. (2004). Minimal nuclear pore complexes define FG repeat domains essential for transport. Nat. Cell Biol. *6*, 197–206.

Sun, Q., Carrasco, Y.P., Hu, Y., Guo, X., Mirzaei, H., Macmillan, J., and Chook, Y.M. (2013). Nuclear export inhibition through covalent conjugation and hydrolysis of Leptomycin B by CRM1. Proc. Natl. Acad. Sci. USA *110*, 1303–1308.

Taura, T., Schlenstedt, G., and Silver, P.A. (1997). Yrb2p is a nuclear protein that interacts with Prp20p, a yeast Rcc1 homologue. J. Biol. Chem. *272*, 31877–31884.

Taura, T., Krebber, H., and Silver, P.A. (1998). A member of the Ran-binding protein family, Yrb2p, is involved in nuclear protein export. Proc. Natl. Acad. Sci. USA *95*, 7427–7432.

Turi, T.G., Mueller, U.W., Sazer, S., and Rose, J.K. (1996). Characterization of a nuclear protein conferring brefeldin A resistance in Schizosaccharomyces pombe. J. Biol. Chem. *271*, 9166–9171.

Wen, W., Meinkoth, J.L., Tsien, R.Y., and Taylor, S.S. (1995). Identification of a signal for rapid export of proteins from the nucleus. Cell *82*, 463–473.

Yang, W., Gelles, J., and Musser, S.M. (2004). Imaging of single-molecule translocation through nuclear pore complexes. Proc. Natl. Acad. Sci. USA *101*, 12887–12892.